EFDA–JET–CP(12)02/14

T. Eich, B. Sieglin, A Scarabosio, A Herrmann, A Kallenbach, G.F. Matthews, S. Jachmich, S Brezinsek, M. Rack, R.J. Goldston, ASDEX Upgrade Team and JET EFDA contributors

Empirical Scaling of Inter-ELM Power Widths in ASDEX Upgrade and JET

Empirical Scaling of Inter-ELM Power Widths in ASDEX Upgrade and JET

T. Eich[1], B. Sieglin[1], A Scarabosio[1], A Herrmann[1], A Kallenbach[1], G.F. Matthews[2], S. Jachmich[3], S Brezinsek[4], M. Rack[4], R.J. Goldston[5], ASDEX Upgrade Team[1] and JET EFDA contributors*

JET-EFDA, Culham Science Centre, OX14 3DB, Abingdon, UK

[1]Max-Planck-Institut für Plasmaphysik, Teilinsitut Greifswald, EURATOM-Assoziation, D-17491 Greifswald, Germany
[2]EURATOM-CCFE Fusion Association, Culham Science Centre, OX14 3DB, Abingdon, OXON, UK
[3]Association "EURATOM - Belgian State" Laboratory for Plasma Physics Koninklijke Militaire School-Ecole Royale Militaire Renaissancelaan 30 Avenue de la Renaissance B-1000 Brussels Belgium
[4]IEK-4, Forschungszentrum Jülich, EURATOMassociation, Germany
[5]Princeton Plasma Physics Laboratory, James Forrestal Campus, Princeton, NJ 08543, New Jersey, USA
** See annex of F. Romanelli et al, "Overview of JET Results", (23rd IAEA Fusion Energy Conference, Daejon, Republic of Korea (2010)).*

Preprint of Paper to be submitted for publication in Proceedings of the 20th International Conference on Plasma Surface Interactions , Eurogress, Aachen, Germany 21st May 2012 - 25th May 2012

Abstract

The SOL power decay length (λ_q) deduced from analysis of fully attached divertor heat load profiles from two tokamaks, JET and ASDEX Upgrade with carbon plasma facing components, are presented. Interpretation of the target heat load profiles is done by using a 1D-fit function which disentangles the upstream λ_q and an effective diffusion in the divertor (S), the latter essentially acting as a power spreading parameter in the divertor volume. It is shown that the so called integral decay length λ_{int} is approximatively given by $\lambda_{int} \approx \lambda_q + 1.64 \times S$. An empirical scaling reveals parametric dependency $\lambda_q/\mathrm{mm} \simeq 0.9 \cdot B_T^{-0.7} q_{cyl}^{1.2} P_{SOL}^{0} R_{geo}^{0}$ for type-I ELMy H-Modes. Extrapolation to ITER gives $\lambda_q \simeq$1 mm. Recent measurements in JET-ILW and from ASDEX Upgrade full-W confirm the results. A regression for the divertor diffusion S is not yet achieved due to the large effect of different divertor geometries of JET and ASDEX Upgrade.

1 Introduction

Operation in diverted high confinement mode (H-Mode[1]) is the foreseen scenario for next step tokamak fusion devices. H-mode plasmas develop an edge transport barrier close to the magnetic boundary separating the closed-field-line region from the open-field-line region or scrape-off-layer (SOL). Operation in H-mode is accompanied by periodic relaxation phenomena called edge-localised-modes (ELMs)[2]. The power decay length, λ_q, in the SOL region is a crucial quantity concerning the divertor peak heat load (q_{max}) for current and future devices.

Infrared camera systems with a target resolution of 1.7 mm and framing rates of about 10 kHz are employed for both devices. Energy effluxes due to ELMs[3] are observed to impose toroidally asymmetric heat flux (q) patterns on the di-

vertor target[4–6] and larger power decay lengths[7]. Additionally as shown in Fig.1, radial movements of the strike line on target, with amplitudes reaching up to the power decay length itself, are observed in JET plasma discharges modulated by ELM induced energy and particle losses[8]. Taking both effects together, time averaged estimates of λ_q covering the complete ELM cycle give too large absolute numbers and different parameter dependency[9]. Thus, to reach improved accuracy, inter-ELM periods from 90% to 99% of the ELM cycle time are defined, removing any influences from the latter effects. The heat flux between ELMs and that during ELMs are due to different physical processes. Only by examining them separately can the processes be understood and scaled to future devices.

The same phenomenology is observed in AUG, though with much reduced amplitudes of less than 5mm[10]. A typical example for ASDEX Upgrade power load evolution during type-I ELMy phase is shown in Fig.2.

2 Database for JET and ASDEX Upgrade

The data base covers 60 deuterium type-I ELMy H-Mode plasmas for JET. For AUG we use values from both, Div-I and Div-IIb, all latter summarised in Table 1. The JET data base is a modest extension of the data base used in [11]. For AUG the numbers of analysed discharges was extended from 11 to 26 H-Mode plasmas and including different divertor geometries[12]. No significant changes w.r.t. [11] are detected.

We denote plasma current as I_p, toroidal magnetic field as B_T, edge safety factor as q_{95}, heating power as P_h, averaged triangularity as δ, effective charge as Z_{eff} and Greenwald density fraction as n_{GW}. The aspect ratio of both machines, defined as $\epsilon = a/R_{geo}$, is $\epsilon = 0.32$, with the major geometrical radius

denoted as R_{geo} and the minor radius as a. The plasma elongation amounts to $\kappa = 1.8$ for both devices. Heat flux profiles are analysed with minimal gas puffing and in the absence of power detachment with carbon divertor plasma-facing components. However, it should be noted that the divertor geometries for JET and ASDEX Upgrade are quite different. JET imposes an open divertor geometry, i.e. the outer strike line is positioned on the outer horizontal target tile[13]. Addionally for JET, only such discharges can be analysed with IR due to the observation geometry (for details see [7]). ASDEX Upgrade Div-IIb runs regularly with both strike points on vertical tiles and establishes this way a more closed, ITER like divertor magnetic configuration[14]. However, AUG Div-I did establish a more open divertor geometry with both strike lines on the horizontal plates[12].

3 Experimental estimation of the power decay length

The SOL power decay length is determined by analysis of heat flux profiles measured on the outer divertor target by means of infrared thermography. Details of the experimental setup for JET can be found in Ref.[7] and for AUG in Ref.[15]. In order to relate the surface heat flux profile to the outer midplane separatrix region, the magnetic flux expansion, f_x, has to be taken into account. We use the definition for an integral flux expansion along the target surface[15,16] calculated for the outer midplane region $R = R_{sep}$ to $R = R_{sep} + 5\,\mathrm{mm}$, with R_{sep} being the outer separatrix radius. The variation of f_x by using $R = R_{sep} + 2.5\,\mathrm{mm}$ amounts to $<5\%$.

This simple ansatz allows to account for perpendicular heat diffusion or *leakage* into the private-flux-region (PFR) by introducing a Gaussian width S representing the competition between parallel and perpendicular heat transport in the divertor volume. This means that, physically, the exponential profile at the divertor entrance[17], is diffused into the private flux region while travelling towards the target[18]. This competition is approximated by a convolution of the exponential profile with a gaussian function with the width S [19]. The target heat flux profiles are thus expressed in a domain s element of $[-\infty, \infty]$.

$$q(\bar{s}) = \frac{q_0}{2} \exp\left(\left(\frac{S}{2\lambda_q}\right)^2 - \frac{\bar{s}}{\lambda_q f_x}\right) \cdot \operatorname{erfc}\left(\frac{S}{2\lambda_q} - \frac{\bar{s}}{S f_x}\right) + q_{BG} \tag{2}$$

Figure 3 shows examples for measured heat flux profiles and fitting results by using Eq.2 with the free constant parameters $S, \lambda_q, q_0, q_{BG}$ and s_0.
Figure 4 shows the resulting values for λ_q and S from fitting for the complete data base. Most notable here is that the values for S are largely varying and seem to cluster for each single divertor around a mean value. In particular it should be noted that for AUG Div-I and Div-IIb largely different values for the power spreading parameter S are found. In contrast λ_q for both devices cover the same range from values of about 1mm to 4mm. Hence, in the JET machine with about 3 meter large radius, shortest power fall-off length of about 1mm are present for highest currents. Also, values of about 1mm to 4mm are found for ASDEX Upgrade, a truly notable result.

4 Comparison of fit results to 2D-modelling of heat transport

Two-dimensional numerical heat diffusion calculations [20] using Spitzer-like ($\propto T^{5/2}$) parallel and Bohm-like perpendicular ($\propto T$) thermal diffusivities show that this technique is accurate to better than 15% in determining λ_q at

the divertor entrance in cases where ratio of the deduced Gaussian width (S) and the exponential fall-off length (λ_q) is below unity as shown in Figure 5. For the mean value of all JET data we get $S/\lambda_q = 0.4$ corresponding to 2% accuracy and for ASDEX Upgrade $S/\lambda_q = 0.57$ corresponding to 5% accuracy.

5 Approximative relation between λ_{int}, λ_q and S

From Eq.2 follows the integral power decay width[16]

$$\lambda_{int} = \frac{\int (q(s) - q_{BG}) ds}{q_{max}} \cdot f_x^{-1} \tag{3}$$

This quantity is frequently used in the literature [16] since it allows to relate the peak heat load on the divertor target to power deposited on the divertor target, a crucial design parameter for the power handling capabilities of a large device such as ITER. It is shown by Makowski that, given the model for the target heat flux from Eqn.2 is applicable, the following relation is accurate to better than 3% for the analysed data base[21]:

$$\lambda_{int} \simeq \lambda_q + 1.64 \cdot S \tag{4}$$

Figure 6 shows a comparison between the experimental integral decay length λ_{int} (see Eqn.3) and the result of the fitting of λ_q and S. The very good correlation confirms the latter approximative relation in Eqn.4. It shows that despite its simplicity the fitting function as stated in Eqn.2 is remarkably well distinguished to characterize the experimentally measured heat load profiles. The most notable conclusion from Eqn.4 is certainly that a regression of λ_{int} as a substitute for λ_q as attempted in earlier studies [16] will necessarily not reveal the correct scaling parameters.

This becomes more evident when having a closer look on typcial values of λ_{int} for AUG Div-I and AUG Div-IIb and comparing them to λ_{int} values from JET. Regressing Div-I and JET data for λ_{int} would give positive major R dependencies, but regressing Div-IIb and JET data would give negative major R dependencies. As stated, this is in both cases an artifact from using λ_{int} rather than λ_q.

6 Multi parameter regression

We provide here empirical regressions for λ_q for JET and for the combined data set from JET and AUG deuterium discharges. A regression for AUG is attempted despite the comparably poor variation in I_p and B_T. Hence only a poor regression quality is found with large error bars for each regression variable. The regression parameters are B_T, cylindrical safety factor (q_{cyl}), power crossing the separatrix (P_{SOL}) and R_{geo} when regressing combined data from both devices. We apply least square fitting to derive a parametric dependency

$$\lambda(\mathrm{mm}) = C_0 \cdot B_T^{C_B}(\mathrm{T}) \cdot q_{cyl}^{C_q} \cdot P_{SOL}^{C_P}(\mathrm{MW}) \cdot R^{C_R}(\mathrm{m}) \tag{5}$$

and use the cylindrical safety factor expressed by

$$q_{cyl} = \frac{2\pi a \cdot \epsilon \cdot B_T}{\mu_0 \cdot I_p} \cdot \frac{(1+\kappa^2)}{2} \tag{6}$$

Results are summarised in Table 2 for λ_q including the regression variances for each variable. For completeness we note that regressions with q_{95} and q_{cyl} give identical dependencies within the error bars.

Table 2

Parameter dependency of λ_q using Eqn.5

Here we point on the main finding that λ_q has a strong dependency on B_T and q_{cyl}, minor dependency on P_{SOL}. Notably no dependency of λ_q on R_{geo} is detected. The regression for the both devices JET and ASDEX Upgrade show the same parameter dependencies within the errorbars. These results are also in line with the results from the combined scaling for D3D, C-Mod and NSTX [21,22] as shown in the table. A comparison of the regressed versus the measured values are given in Fig.7 for JET, ASDEX Upgrade Div-I and Div-IIb.

7 First results from 'tungsten' divertor operation in JET and ASDEX Upgrade

Recent experiments in JET-ILW plasmas[23] with dedicated scans in plasma current (1-2.8MA)and toroidal field (1-2.5T) to assess the empirical scaling provide confirmation of the latter results. Also ASDEX Upgrade low density discharges at 1.2MA, 2.5T, 12.5MW NBI and 3MW ECRH heating with the full tungsten wall[24] are fully in line with the empirical scaling as presented in Fig.7. Note that the divertor geometry of full-W AUG operation is nearly identical to AUG Div-IIb.

8 Comparison to the power fall-off with in L-Mode plasmas

The presented studies were recently extended for dedicated L-Mode discharges or short L-Mode phases before transition to H-Mode for both, JET and ASDEX Upgrade. A detailed discussion can be found in [25]. For all cases it is found that $\lambda_{q,L-mode} > \lambda_{SOL,H-mode}$. For most cases $\lambda_{q,L-mode}$ is $2-3$ times larger than predicted by the H-Mode scaling law. This is expected since radial

transport in L-mode is larger than in H-mode in the edge plasma. Slightly different results are achieved for the L-Mode regression of λ_q depending on the chosen data base from JET and AUG as no dedicated scans for L-Mode plasmas, in contrast to the H-Mode studies, are available. The best results w.r.t. best regression residuals from least square fitting for a combined JET and AUG data base are:

$$\lambda^{L-Mode}(\mathrm{mm}) = 1.37 \cdot B_T^{-0.55}(\mathrm{T}) \cdot q_{cyl}^{1.17} \cdot P_{SOL}^{0.2}(\mathrm{MW}) \cdot R^{0.1}(\mathrm{m}) \tag{7}$$

Most worth notifying here is that the L-Mode regression parameter are reminiscent of those found for H-Mode plasmas but with an about 2 times larger constant, hence larger values for λ_q in L-Mode. When extrapolating to ITER for L-Mode plasma by using Eqn.7 and P_{SOL}^{L-Mode}=50 MW a value for λ_q of 3.8 mm is found for ITER. Following the studies in [25] λ_q^{L-Mode} is between 3.4mm and 5.5mm.

Next we look closely at the heat flux profiles during a selected L-H transition for a JET deuterium plasma. The NBI power step-up initiates a fast electron pedestal temperature increase. After about 100ms the heat flux channel λ_q is reduced by about a factor of 2. After another 200ms λ_q has reached its ELM-free H-mode value which is in line with inter-ELM scaling for H-Modes. Also S decreases by about 30%, possibly due to the increase of the separatrix temperature and consequently increased parallel electron conduction. Analysis of the kinetic evolution of profiles shows notably that the shrinking of the heat flux channel is linked with the changes in the pedestal temperature only. The pedestal density evolves much more slowly and does not show a correlation to the change of λ_q when going from L- to H-Mode operation.

8 Conclusion

9 Conclusions

An approximative expression for the target heat load profiles is introduced. From this expression we are enabled to disentangle the integral (λ_{int}) and exponential (λ_q) power fall-off widths and an effective power spreading parameter (S). A most notable conclusion of the analysis of λ_q is that no machine size scaling is detected. The design values for ITER of interest here are R=6.2 m, a=2.0 m, κ=1.7, P_{SOL}=120 MW, B_{tor}=5.3 T, I_p=15 MA, q_{cyl}=2.42, Z_{eff}=1.6. Extrapolation of the regression analysis from Table 2 results in $\lambda_q^{ITER} \simeq$1 mm.

Recent experiments carried out with 'tungsten' divertors in JET and ASDEX Upgrade revealed no deviations from the results with carbon plasma-facing-components. The comparison λ_q to the prediction of the heuristic drift based model[28], based on parallel convection and curvature drifts, is satisfactory with regard to both magnitude and scaling.

However, extrapolation of λ_{int} to ITER cannot be given from this work. This requires a reliable regression of S from the current data base which is not yet achieved. Such an attempt has to include an understanding of the effect of the divertor geometry on the power spreading S parameter. Also accompanying code simulations seem to be necessary focussing on discharge conditions in absence of detachment processes[29–31].

However, the huge observed difference of the S parameter between ASDEX Upgrade Divertor-I and Divertor-IIb gives hope that a suffiently large S in the long baffled ITER divertor will be present and hence will cause $\lambda_{int} >> \lambda_q$. As an exercise only for curiosity we use the S value from ASDEX Upgrade Div-IIb and calculate λ_{int} for ITER

$$\lambda_{int}^{ITER}(\text{mm}) = 1mm + 1.64 \times 1.6mm = 3.6mm >> 1mm \quad (8)$$

We note that in case that S is large enough, the actual λ_q could be of minor importance. Only dedicated experiments aiming to find a scaling of S, can lead to a better understanding here, e.g. by varying the distance between x-point and divertor target plate in controlled experiments with otherwise fixed discharge parameters (i.e. constant λ_q) as executed in DIII-D [32] recently.

ITER is anticipated to operate in conditions with a high fraction of SOL radiation and partially detached divertor plasmas, unlike the conditions studied here. However, the assumption [33] that λ_q will be in the range of 5 mm needs to be compared to consequences for operation and divertor detachment accessibility arising from the prospected result of $\lambda_q \approx 1mm$, as aimed for in [34]. We finally note that the results here from simple regression analysis are not constrained by other effects which may be present and would be violated by a power fall-off length of 1mm in the outer midplane in ITER [35].

Acknowledgements

The authors want to thank O.Kardaun, T.Pütterich and C.Lowry for support and discussions. In particular we like to thank A.W.Leonard and M.Makowski from DIII-D and J.Terry from Alcator C-Mod for highly valuable discussion. Further credit is paid to the support of the IR team in JET, i.e. S.Devaux, G.Arnoux and I.Balboa and P.de Marne from ASDEX Upgrade. This work was supported by EURATOM and carried out within the framework of the European Fusion Development Agreement. The views and opinions expressed herein do not necessarily reflect those of the European Commission.

References

[1] F. Wagner *et al.*, Phys. Rev. Lett. **49**, 1408 (1982).

[2] D. Hill *et al.*, J.Nucl.Mater. **241-243**, 182 (1997).

[3] A. Loarte *et al.*, J.Nucl.Mater. **313-316**, 962 (2003).

[4] T. Eich, A.Herrmann, J.Neuhauser, Phys.Rev.Letter **91**, 195003 (2003).

[5] S. Devaux *et al.*, J.Nucl.Mater. **415**, S865 (2011).

[6] A. Wingen, T.E.Evans, C.J.Lasnier, K.H.Spatschek, Phys.Rev.Letter **104**, 175001 (2010).

[7] T. Eich *et al.*, J.Nucl.Mater. **415**, S856 (2011).

[8] E. Solano *et al.*, Nuclear Fusion **48**, 065005 (2008).

[9] W. Fundamenski *et al.*, Nuclear Fusion **45**, 950 (2005).

[10] M. Dunne *et al.*, submitted to Nuclear Fusion

[11] T. Eich, *et al.*, Phys.Rev.Letter **107**, 215001 (2011).

[12] A.Herrmann *et al.*, Fusion Science Technology **44**, 569 (2003).

[13] S. Brezinsek *et al.*, J.Nucl.Mater. **415**, S936 (2011).

[14] A. Kallenbach *et al.*, J.Nucl.Mater. **415**, S19 (2011).

[15] A. Herrmann *et al.*, Plas.Phys.Contr.Fus. **44**, 883 (2002).

[16] A. Loarte *et al.*, J.Nucl.Mater. **266-269**, 587 (1999).

[17] P. Stangeby *et al.*, Nuclear Fusion **50**, 125003 (2010).

[18] A. Loarte *et al.*, Contrib. Plasma Phys. **32**, 468 (1992).

[19] F. Wagner, Nucl. Fusion **25**, 525 (1985).

[11] T. Eich, *et al.*, Phys.Rev.Letter **107**, 215001 (2011).

[12] A.Herrmann *et al.*, Fusion Science Technology **44**, 569 (2003).

[13] S. Brezinsek *et al.*, J.Nucl.Mater. **415**, S936 (2011).

[14] A. Kallenbach *et al.*, J.Nucl.Mater. **415**, S19 (2011).

[15] A. Herrmann *et al.*, Plas.Phys.Contr.Fus. **44**, 883 (2002).

[16] A. Loarte *et al.*, J.Nucl.Mater. **266-269**, 587 (1999).

[17] P. Stangeby *et al.*, Nuclear Fusion **50**, 125003 (2010).

[18] A. Loarte *et al.*, Contrib. Plasma Phys. **32**, 468 (1992).

[19] F. Wagner, Nucl. Fusion **25**, 525 (1985).

[20] R. Goldston, Physics of Plasmas **17**, 012503 (2010).

[21] M. Makowski, Physics of Plasmas **in print**, 000000 (2012).

[22] R.Maingi *et al.*, these proceedings

[23] G. Matthews *et al.*, these proceedings

[24] R. Neu *et al.*, these proceedings

[25] A. Scarabosio *et al.*, these proceedings

[26] A. Kallenbach *et al.*, Plas.Phys.Con.Fus. **46**, 431 (2004).

[27] W. Fundamenski *et al.*, Nucl.Fusion **51**, 083028 (2011).

[28] R. Goldston, Nuclear Fusion **52**, 013009 (2012).

[29] M. Wischmeier *et al.*, J.Nucl.Mater. **415**, S523 (2011).

[30] B. Lipschultz *et al.*, J.Nucl.Mater. **241-243**, p.771 (1997).

[31] M. Fenstermacher *et al.*, Plas.Phys.Con.Fus.. **41**, A345 (1999).

[32] T.W. Petrie *et al.*, these proceedings

[33] ITER Phys. Exp. Group, Nucl.Fusion **47**, S203 (2007).

[34] A. Kukushkin *et al.*, these proceedings

[35] D. Whyte *et al.*, these proceedings

Data base of analysed discharges

	#	I_p[MA]	B_T[T]	q_{95}	P_h[MW]	δ	Z_{eff}	n_{GW}
JET	60	1.0-3.5	1.1-3.2	2.6-5.5	5-24	0.2-0.4	1.5-2.5	0.44-0.88
AUG Div-IIb	22	0.8-1.0	1.5-2.4	3.2-5.1	2.5-12.5	0.2-0.4	2.0-2.7	0.46-0.74
AUG Div-I	4	1.0-1.2	1.9-2.0	2.6-3.0	5.0-7.5	≈0.1	-	≈0.5

Table 1:

Parameter dependency of λ_q using Eqn.5

			C_0	C_B	C_q	C_P	C_R	R^2
JET	λ_q		0.70	-0.85	1.23	0.13	-	0.68
		$\pm$	0.23	0.26	0.24	0.12	-	
AUG	λ_q		0.78	-0.63	1.14	-0.05	-	0.43
		$\pm$	0.69	1.05	0.81	0.31	-	
JET+AUG	λ_q		0.90	-0.73	1.16	0.04	-0.11	0.61
		$\pm$	0.37	0.26	0.27	0.12	0.15	
D3D+NSTX+CMod	λ_q		0.93	-0.97	1.09	-0.10	-	0.79
		$\pm$	0.26	0.06	0.20	0.09	-	

Table 2:

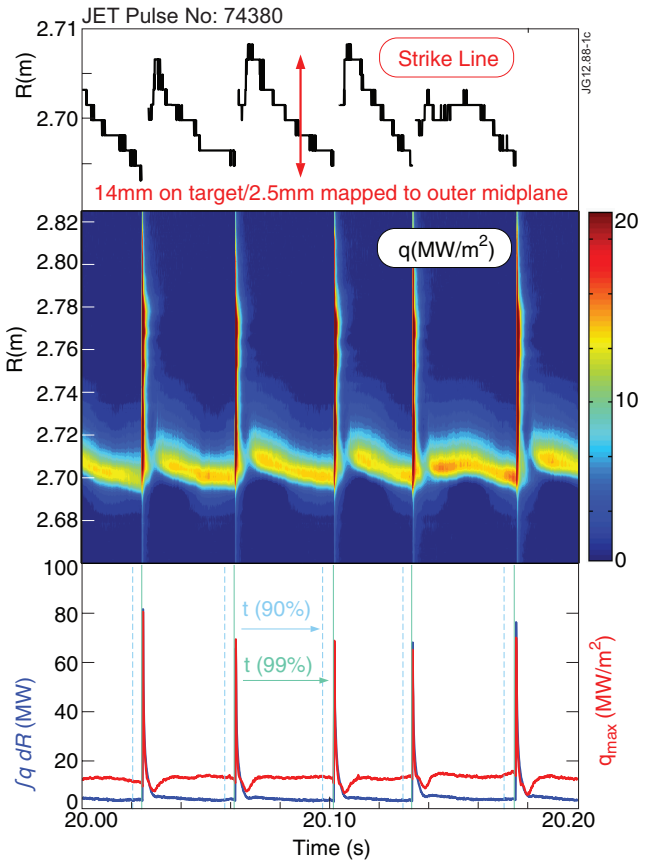

Figure 1: Evolution of heat flux and the inferred strike line position on the divertor target for a typical JET discharge during type-I ELMy phase.

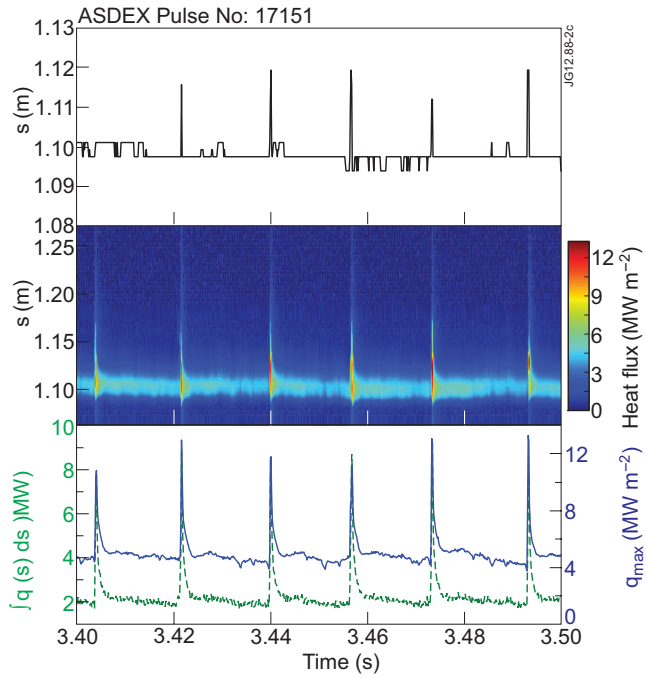

Figure 2: Evolution of heat flux and the inferred strike line position on the divertor target for a typical ASDEX Upgrade discharge during type-I ELMy phase.

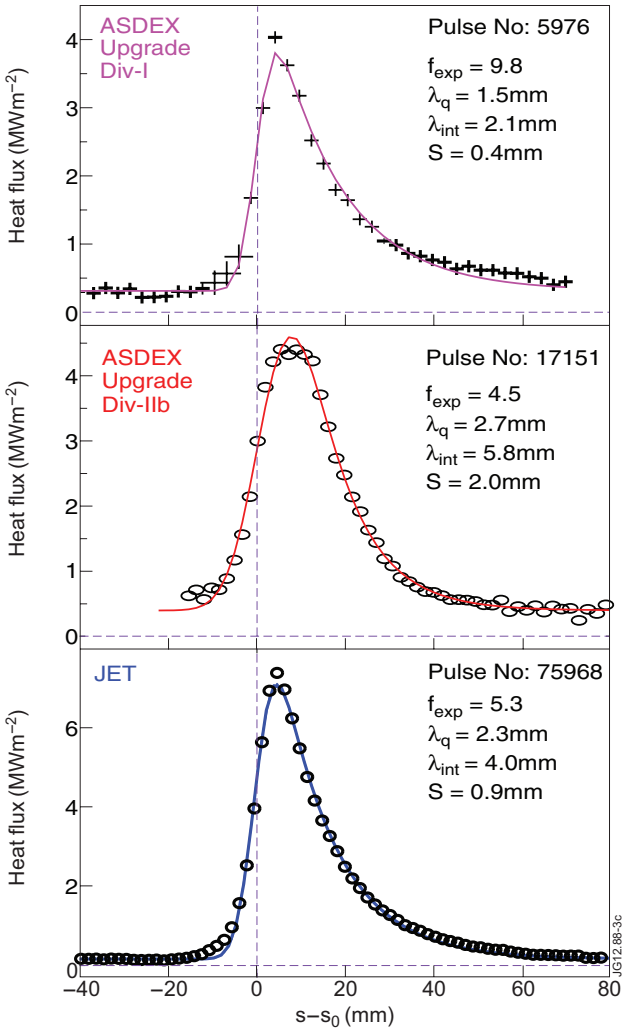

Figure 3: Heat flux profiles measured on the outer divertor target and fits using Eq.2 applied to heat flux data for JET and AUG Div-I and Div-IIb.

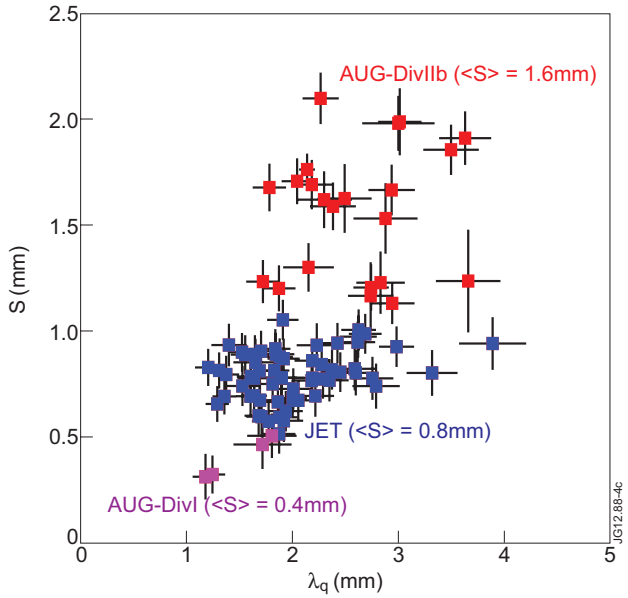

Figure 4: Resulting values for λ_q and S from fitting for the complete data base.

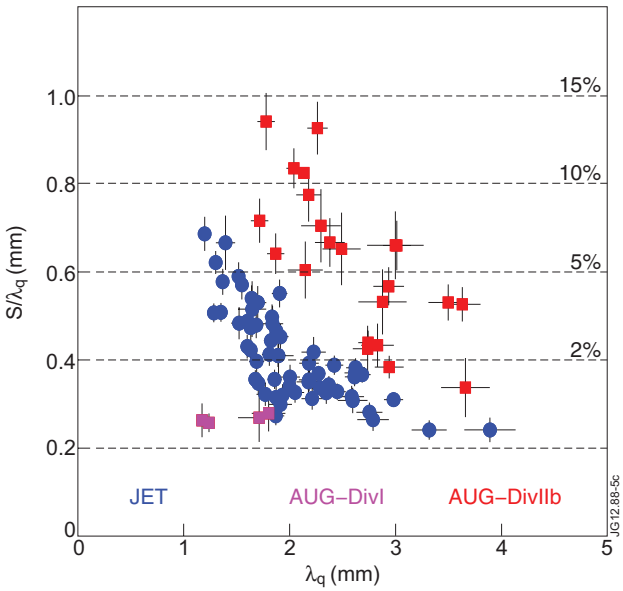

Figure 5: The deviation of using constant diffusion rather than solving the 2D numerical heat diffusion is dependent on S/λ_q and below 6% and 15% for JET and ASDEX Upgrade, respectively.

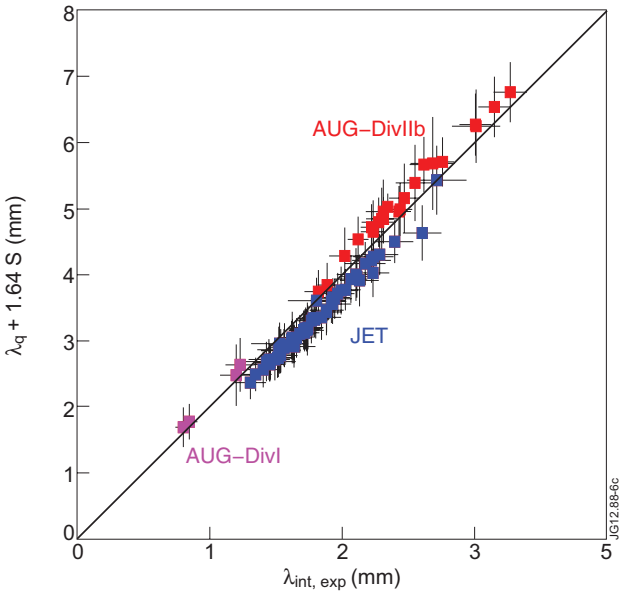

Figure 6: Correlation between the experimental and fitted λ_{int} by λ_q using and S and applying the Makowski relation.

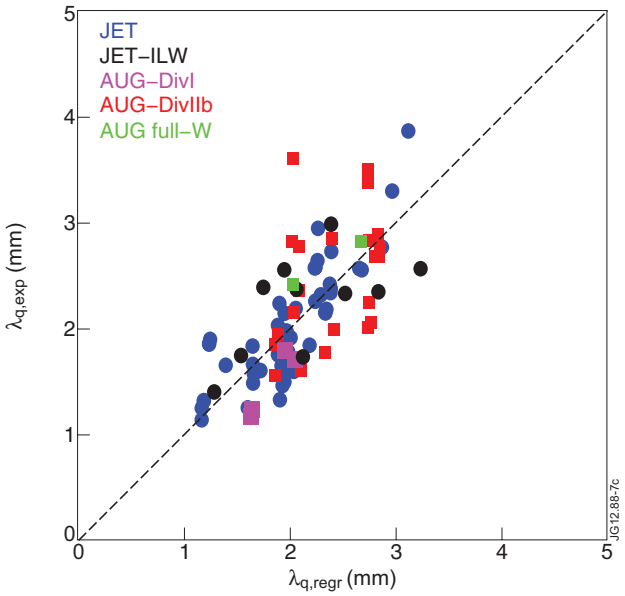

Figure 7: Comparison of predicted (see Table 2) versus measured values for λ_q.